CRITICAL CHARACTERS OF FLY ASH SUPPRESSING ASR

Haruka Takahashi[1], Kazuo Yamada[1*]

[1]Taiheiyo Cement Corp., Sakura, Chiba, Japan (present: Taiheiyo Consultant, Co., Ltd.)

Abstract

Feature analysis of fly ash (FA) was carried out for five different FA (equivalent to JIS Class II) having different alkali-silica reaction (ASR) suppression effect. Then critical chemical and physical characteristics of FA relating their effects are discussed. By using a scanning electron microscope combined with backscattered electron detector, energy dispersive X-ray spectrometer and electron backscattered diffraction detector, it revealed that FA is composed of not only several mineral phases and single amorphous phase as estimated by X-ray diffraction but also several types of amorphous phases with complicated textures. Feature analysis classified them into six phases quantitatively and gave particle size distribution and specific surface area of each phase. Among them, a kind of particles in which needle-like mullite particles are dispersed in amorphous silica-rich matrix showed a strong negative correlation with mortar bar expansion containing different FA. This suggests that specific surface area of these particles is critical for the ASR suppressing effect of FA.

Keywords: Fly ash, Feature analysis, Backscattered electron image, Electron backscatter diffraction, Suppressing ASR

1 INTRODUCTION

Fly ash (FA), which is produced as an industry by-product, is utilized as one of supplementary cementitious materials (SMC). As effects of FA mixing, some improvements are achieved, such as increase of long-term strength and decrease of heat of hydration. Furthermore, it is well known that FA concrete where fly ash is mixed suppresses the alkali-silica reaction (ASR). From this viewpoint, there have been many reports demonstrating that FA concrete acts as an essential measure to prevent ASR deterioration. However, since the suppressing effect of ASR differs depending on the characteristics of FA, the required volume to show effective ASR suppression is known to vary depending on the quality of FA [1].

As the indices of the suppressing effect of ASR, various parameters are used, such as the amount of amorphous phase in FA, the amount of amorphous silica, the chemical composition (basicity, etc.), and physical characteristics (Blaine specific surface area, etc.) [2-5]. However, any indices are not sufficiently applicable to investigate the suppressing effect of ASR for a wide range of FA sources. Therefore, it is needed to perform detailed examination of the relation between the suppressing effect of ASR and FA characteristics, that is, characterization of FA in terms of what kinds of FA particles having what kinds of characters actually contribute to the suppressing effect of ASR.

Several examples of FA characterization have been reported, where FA particles were classified by analysis results of chemical composition and elemental mapping obtained by point analysis or area analysis using a field-emission scanning electron microscope (FE-SEM) equipped with an energy dispersive X-ray spectrometer (EDS) [6-8]. These reports strongly indicate that FE-SEM enabling high-magnification observation is effective for micro texture in FA fine particles.

* Correspondence to: kazuo_yamada@taiheiyo-cement.co.jp

However, these studies are confined to classification of FA particles and do not examine physical characteristics of hardened cement paste, especially the relation with the suppressing effect of ASR which is the main purpose of the present study.

In the field of metal/iron and steel, characterization using FE-SEM is popular for general-purposes. Along with recent progress of computational technology, FE-SEM equipped with a detector of electron backscatter diffraction (EBSD) has been used for many studies of crystal analysis [9,10]. EBSD performs crystal structure analysis based on Kikuchi line diffraction patterns (EBSD patterns) obtained from crystalline particles. The analysis depth of EBSD is as small as 30~50 nm, thus enabling information on top-surface layers of the specimen and high special resolution at least 100 μm to be obtained. Thus, SEM-EBSD is expected to be used as an effective tool for feature analysis of FA, as well as SEM-EDS.

In recent years, in order to detect inclusions or precipitates, FE-SEM has been used for feature analysis in the metal/iron and steel fields [10]. Feature analysis is a method of particle image analysis by extracting and separating target particles from secondary electron (SEM) images or backscattered electron (BSE) images and elemental mapping images. By performing EDS analysis of particles extracted from BSE or SEM images, it is possible to statistically analyze not only geometrical parameters (area, boundary length, degree of circularity, aspect ratio, etc.) but also chemical composition. If target analysis objects can be sufficiently separated and extracted from BSE or SEM images, the feature analysis is also expected to play a significant role as a new quantification method in the filed of cement and concrete.

Under this circumstance, in this study, FE-SEM/ EDS-BSE-EBSD is used for FA characterization, and feature analysis is carried out for different FA in terms of physical and chemical characteristics. Classification based on quantitative values (feature amounts) that characterize differences in FA particles is conducted to examine the relation between FA characteristics and the suppressing effect of ASR.

2 EXPERIMENTS

2.1 FA characteristics

Five different FA (equivalent to JIS Class II) produced at different thermal power plants were used. Tables 1, 2, 3 and 4 respectively show the chemical compositions by X-ray florescence analysis (XRF) using calibration curves, the mineral compositions by the powder X-ray diffraction (XRD) /Rietveld method (Rietveld analysis) [12], the chemical composition of amorphous phases in the FA and physical characteristics. For XRD measurements, 10 mass% of α-alumina was mixed as an internal standard. Measurement condition of XRD is CuKα as a target, 50kV of accelerating voltage, 350 mA of current, 5~65° (2θ) of scanning range, 0.0234° of step width, 0.13 s/step of scan speed. TOPAS (Bruker AXS) was used as a software for Rietveld analysis. Calculated phases are α-quartz, mullite, magnetite, hematite, lime, gypsum and internal standard of α-alumina. The amount of amorphous phase was calculated by Equation 1.

$$G=100\times(A-R)/(A\times(100-R)/100) \quad (1)$$

G: Amorphous phase amount, A: Measured amount of corundum, R: Added ratio of corundum.

The chemical composition of amorphous phase in FA was calculated by the depletion of the chemical composition based on the mineral composition obtained by Rietveld method from the total chemical composition obtained by XRF. CaO content of every FA was low as less than 5 mass% and alkali content was also less than 1.5 mass%. Chemical compositions as a whole or amorphous phase were similar excepting FA-d and the Blaine surface are was limited in the range of 3490~3890 cm²/g.

In Fig. 1, the particle size distribution of FA measured by Laser diffraction/ scattering method is shown. Although the Blaine specific surface areas of each FA were comparable, their particle size

distributions were considerably different. Median diameters of each FA were shown in Table 4. According to JIS A Class 6201 Annex 2, the pozzolan activity indices of the five FA were obtained from FA-mixed mortar materials based on the compressive strength at the ages of 28 days and 91 days. The obtained results of each index are shown in Table 4. The activity indices were almost same for every FA.

2.2 Suppressing effect of ASR in FA

ASTM C 1260 is basically used to detect potential alkali silica reactivity of aggregate. The application of this method can be extended to evaluate the suppressing effect of ASR by pozzolan including FA [13]. In this study, because it is possible to evaluate ASR suppressing effects in relatively rapidly and water curing at 80 ºC can accelerate pozzolanic reaction of FA, it was considered possible to evaluate the effect of FA characteristics and ASTM C 1260 was adopted.

In this study, cements used were ordinary Portland cement and FA blended cements having replacement ratios of 5, 10, and 20 mass%. The fine aggregate used was a highly alkali reactive crushed sand of two-pyroxene andesite from Hokkaido containing volcanic glass, cristobalite and tridymite as reactive mineral phases. Chemical method according to JIS A 1145 showed harmless as Sc=532 > Rc=115. The mortar bar method according to JIS A1146 showed also harmless as 0.5% expansion in 3 months. These two materials were used to prepare mortar specimens. Sealed curing was carried out for 24 hours after mixing, and then demolded and specimens were cured under water at 80 ºC for 24 hours. Finally, the length after curing was taken as the gauge length. After that, the mortar specimens were immersed in a NaOH solution of 1 mol/L (80 ºC) for 14 days. As a result, the expansion ratio (14 d expansion ratio) of the specimen was used as an index of the suppressing effect of ASR. In Figure 2, the relation between the FA replacement ratio and the 14 d expansion is shown.

At FA replacement ratio of 20 mass%, ASR expansion was effectively suppressed and no difference was found among the five FA, but at less substitution ratios, the suppressing effects of ASR were different. FA-d was most effective even in low replacement ratio. There were no significant correlations between amorphous amount that were considerably different among FA or specific surface area calculated from particle size distribution and 14 d expansion.

2.3 Observation using FE-SEM and feature analysis of FA

Specimen preparation

To observe crystal phases and amorphous phases in FA, an FA-polished specimen was prepared by using the Cross Section Polisher™(JEOL SM-09020), which etches a specimen surface with an Ar ion beam and produces a polished surface with little milling distortion even for a relatively soft material.

The procedures for specimen polishing are as follows. First, FA and low-viscosity epoxy resin were mixed with a weight ratio of 1:1, and the resin-mixed specimen was poured into a 1-inch cylindrical ring. After the resin was hardened, this specimen was cut to a size of 5×5×2 mm. Then, the Cross Section Polisher was used to polish it (accelerating voltage: 6 keV, milling time: 10 hours). After that, in order to give conductivity to the specimen, the specimen was coated with carbon (thickness: about 5 nm).

BSE image observation, EBSD analysis and elemental analysis by EDS

The difference of gray level in BSE image depends on the average atomic number of constituent elements in the region where BSE are generated. As this value is larger, the corresponding part appears brighter. Thus, when chemical compositions are different among FA particles, the chemical composition difference is recognized as a difference of gray level. Besides, by using EBSD crystal phases were identified and amorphous phases in FA particles was estimated when EBSD patterns cannot be obtained. In the

present study, FE-SEM used was equipped with BSE and EBSD detectors (JEOL JSM-7001F/ JEOL SM-54060RBEI/ Oxford Instruments HKL Channel 5). Accelerating voltage was 15 keV for BSE observation and 3 keV for EBSD analysis. Observation magnification was adjusted depending on the size of FA particle.

To obtain the chemical composition of crystal and amorphous phases in FA EDS (Oxford instruments, INCA energy) was used for elemental analysis. Accelerating voltage was 15 keV, probe current was 300 pA, working distance was 10 mm and analysis time was 100 s/ point. At this measurement, although the X-ray generation region mainly covers the position close to that of electron beam irradiation, it should be noted that this region may be extended to a range of 2.5~3.0 μm from the beam irradiation position when specimen density and chemical composition are taken into account.

Feature analysis

In Figure 3, a flow diagram of feature analysis is shown. First, a BSE image of FA is acquired and from a gray-level histogram of the BSE image, threshold values to extract the target FA particles are determined. Binary processing is conducted using the threshold values and the FA particles to be analyzed are extracted. The extracted FA particles are automatically numbered by the particle type and EDS chemical analysis is performed for each particle. Next, the FA particles are classified based on geometrical parameters, *i.e.* circularity coefficient, circle-equivalent diameter, and aspect ratio) and chemical compositions obtained from each particle. The threshold values used for classification were determined from the results of BSE images and EBSD patterns and EDS analysis. These threshold values will be described later.

In this study, FE-SEM with BSE/EDS was used and feature analysis was carried out for 1000 points in the five different FA particles according to the above-explained analysis flow diagram. The measurement conditions were as follows; accelerating voltage: 15 keV, probe current: 300 pA, observation magnification: ×1000. In addition, INCA Feature (Oxford Instrument) was used as feature analysis software.

3 RESULTS AND DISCUSSIONS

3.1 Observation and analysis of FA particles by BSE, EBSD and EDS

BSE image observation

FA have different shapes for each particle and also, the brightness of FA (gray level) in BSE image differs for each particle. In addition, the gray levels of some particles are not homogeneous within the particle. Differences in gray level suggest a possibility of the existence of multiple kinds of amorphous phases having different chemical compositions. To obtain the feature amounts of each FA particle, it is essential to firstly know the chemical compositions of crystal phases and amorphous phases. For this purpose, BSE image observation was carried out to confirm the existence status of crystal phases and amorphous phases, which had been detected by Rietveld analysis. Figure 4 shows one example of BSE images. Although Figure 4 is one example, BSE images of other different FA are also similar without shape differences.

The diameters of FA particles observed with a magnification of ×250 broadly ranged in 0.5~100 μm, and the particles had various shapes such as circle, hollow cenosphere, agglomerates, and angular particle. Magnetite detected by Rietveld analysis appeared as the brightest particle (arrow 1 in Figure 4) because of the heavy iron. As for the other particles, although their gray levels were recognized to be slightly different, mullite and α-quartz were not distinguished only by the gray level difference in BSE images.

EBSD observation and EDS elemental analysis

It is impossible to distinguish crystal and amorphous phases only with BSE. In order to gain more information on crystal structures and composition, EBSD and EDS analyses were carried out. In Figures 5 and 6, BSE images and EBSD patterns of each FA particle and EDS spectra of these particles are shown, respectively. In the BSE images, EBSD and EDS analysis points are respectively indicated by (+) and (×).

Particles which were estimated to be magnetite in BSE images as they appeared bright (indicated by

arrow 1 in Figure 4 and in Figure 5(a), (b)) were confirmed to be hematite or magnetite from EBSD patterns. Since the amount of hematite was low, it might not be detected by Rietveld analysis. From the EDS elemental analysis result (Figure 6, hematite analysis point 1), it was revealed that Si and Al were slightly detected as well as Fe. From the low gray-level part in the same particle, no EBSD pattern was acquired and amorphous material (phase), as the matrix, was considered to combine with hematite. This point was subjected to EDS analysis and Si and Al were detected with a small amount of Fe (Figure 6, hematite analysis point 2). When scattering effects of an incident electron beam was taken into account, it was estimated that Fe peak is generated due to the influence of hematite and the main chemical compositions of the amorphous part are SiO_2 and Al_2O_3.

In FA particles having an average gray level, needle-like crystal phases were recognized (Figure 5(c)). This was confirmed to be mullite from the EBSD analysis result. In the same particle, from a matrix part having a lower gray level near mullite, no EBSD pattern was acquired; therefore, it was estimated that mullite particles also combine with amorphous phases. In the EDS qualitative analysis result of mullite (Figure 5 (c), mullite analysis point 1), Al_2O_3 content was more than SiO_2 and in it of amorphous matrix (Figure 5 (c), mullite analysis point 2), the concentration of SiO_2 and Al_2O_3 was almost the same or that of SiO_2 was slightly higher. When taking account of scattering effects of an incident electron beam, SiO_2 may mainly dominate the chemical composition of the amorphous part.

An angular particle, as shown in Figure 5 (d), was identified to be α-quartz. The observation result in Fig. 5(d) and Fig. 4 (arrows 2(a), (b)) showed several forms of α-quartz existence; a single crystal or existed with amorphous phases in a fusion form. In the EDS analysis of this particle (Figure 6, α-quartz), the amount (quantitative value) of SiO_2 showed more than 95 mass% and other elements were not detected.

Furthermore, EBSD analysis was performed for FA particles that show the same or slightly higher brightness compared to the particles containing mullite (Figure 5 (e), (f)). In this analysis, no EBSD pattern was acquired, thus these were estimated as amorphous. From the EDS analysis (Amorphous 1), the existence of Si and Al were confirmed from the particles in Figure 5 (e). On the other hand, from the EDS analysis (Amorphous 2), Si, Al and Ca were detected from Figure 5 (f). It was thought that the particles containing Ca show a higher gray level due to the larger atomic weight of Ca.

When reviewing the BSE/EBSD/EDS observation and analysis results of all the five different FA, the FA particles were classified into the following five kinds. (1) FA particle in which amorphous phases and hematite or magnetite combine, (2) FA particle in which amorphous phases and mullite combine, (3) α-quartz, (4) FA particle 1 composed only of amorphous phases (crystal phase not contained): Al_2O_3-SiO_2 system, (5) FA particle 2 composed only of amorphous phases (crystal phase not contained): Al_2O_3-SiO_2-CaO system. In addition to these five kinds, FA particle containing many Ti was confirmed although this was not found in EBSD observation and one more classification has to be set; (6) FA particle with a high concentration of Ti.

3.2 Feature Analysis

Classification of FA particles

EBSD and EDS analyses were able to classify FA particles into six types. In particular, the quantitative values obtained from the EDS analysis could be utilized as the threshold values for FA particle classification. These threshold values were used as key parameters to quantitatively classify the FA particles. Table 5 shows oxides used for acquiring thresholds and the resultant thresholds. FA particles in which amorphous phases and hematite or magnetite are mixed showed more than 25 mass% of Fe_2O_3, and also FA particles containing TiO_2 showed more than 25 mass% of TiO_2; therefore, particles that satisfied the range of the former and latter thresholds were respectively classified into Fe-rich particle and Ti-rich particle. FA particles that showed 95 mass% of SiO_2 were classified as α-quartz. FA particles containing mullite were regarded to have SiO_2 and

Al_2O_3 quantitative values of 25 mass%; therefore, the particles corresponding to this range were classified as mullite-rich particle. As for two types of FA particle composed only of amorphous phases, quantitative values of SiO_2 and CaO were focused. In the Al_2O_3-SiO_2 system, SiO_2 showed 25 mass% or more and also Al_2O_3 showed less than 25 mass%; therefore, the particles satisfying this range were classified as Al-Si amorphous. On the other hand, the Al_2O_3-SiO_2-CaO system was regarded to contain CaO more than 25 mass%; therefore, the relevant particles were classified as Al-Si-Ca amorphous.

In Table 6, the number of FA particles classified by the above-described criteria is shown. The number of FA particles that did not satisfy the criteria was only less than 1% of the total and they are negligible. When the ratio of the number was compared among the five different FA, FA-c has the largest number of mullite-rich particles and FA-a, d, and e contain many Al-Si amorphous particles.

Feature amounts of each classified phase

In the ratio of the number of the classified FA particles, differences were found among the five different FA. To obtain more details of the feature amounts of the classified FA, the FA particle size distribution was estimated using the Shwaltz-Saltykov method [14,15] based on the circle-equivalent diameters of the FA particles obtained by feature analysis. By this method, from the circle equivalent radius distribution of particles appeared in 2D cross section, radius distribution in 3D space is estimated by probabilistic calculation. When particle size 0~Dmax is divided equally by arbitrary range (Δ), the possibility of a particle having a diameter Dj produces circle cross section having diameter Di ($\Delta \leq i \leq j \leq max$) is calculated. The number of particles having diameter Di per unit surface area is equal to the possibility "of each particle having diameter Di~Dmax (particle size increases by Δ) to show circle cross section Di" multiplied with particle number of diameter Di per unit volume. The particle number of diameter Di identified per unit area is known and the number of particle having diameter Di is calculated and particle size distribution is obtained. It is possible to calibrate shifting of particle size distribution to smaller side when equivalent circles area appeared in 2D cross section is assumed to be true particle size.

Focusing on the amorphous phase that is estimated to influence the suppressing effect of ASR, the estimation was conducted. In Figure 7, the estimated particle-size distribution mullite-rich particles are shown. From this estimation, the average particle size, particle volume fraction and specific surface area of each phase were calculated and shown in Table 7. Regarding Al-Si-Ca amorphous particles, the number of particles was small and they were ignored. The estimated values of particle size for Al-Si amorphous particles were similar to each other except for FA-b. In the estimation of mullite-rich particles, FA-a and FA-e were similar but others showed differences among the five different FA.

Regarding the SEM observation, attention is needed for the fact that too coarse particles and too fine particles under spatial resolution are overlooked. However as a result, the feature analysis in this study gave the following average particle sizes of 1000 points of FA; FA-a: 20 μm, FA-b: 33 μm, FA-c: 40 μm, FA-d: 12 μm and FA-e: 15 μm. The average particle size of the Al-Si amorphous particles were around 10 μm for FA-a, d and e, which showed similar values. However, FA-b showed the largest average particle size of 33 μ m. As for mullite-rich particles, arranging the average particle sizes in descending order resulted in FA-c > FA-b > FA-e ≈ FA-a > FA-d. Although in the cases of FA-b and FA-c, larger particles than 40 μm of diameter on the cross section were observed among 1000 particles, no such particles were identified in other FA. Although the existing possibility of large particles is low, the effect of total volume fraction is significant and the average particles size became larger in the case of FA-b and c.

In Table 7, average particles size and volume of each phase are shown. The density of mullite is assumed to be 3.1 g/cm^3 and the volume was calculated as FA-c = 10.8 vol%, FA-b = 11.4 vol%, FA-c = 10.8 vol%, FA-d = 8.9 vol%, and FA-e = 10.8 vol%. Considering the measurement error of Rietveld methods, the difference among FA is limited. However, the volume fraction of mullite-rich particles showed

significant variation. The reason may be in the volume difference in amorphous phase accompanied.

3.3 Relation between Suppressing Effect of ASR and Feature Amounts of FA

When considering a mechanism for the suppressing effect of ASR in FA, two factors can be pointed out; alkali fixation by C-S-H in low Ca/Si produced from pozzolan reaction and alkali penetration suppressing action due to impermeable pore structure. In the foreign alkali environment such as ASTM C 1260, changing pore structure impermeable may further contribute to the suppressing effect of ASR compared with alkali fixation [16]. Thus, the pozzolan reaction making pore structure more impermeable is caused not only by the amount of amorphous phases in FA, but also by the specific surface area of the phases. Therefore, the specific surface areas of mullite-rich and Al-Si amorphous particles were selected and relation between the suppressing effects of ASR was examined.

At FA substitution ratios of 5 mass% and 10 mass%, a strong negative correlation was confirmed between the specific surface area of mullite-rich particle and the 14-day expansion ratio as shown in Figure 8. To the contrary, Al-Si amorphous particles did not show a clear correlation. This result suggest that amorphous phases contained in mullite-rich particles exhibit a higher reactivity than those in Al-Si amorphous particles and these phases have a strong effect on densification of pore structure. The relation between total porosity measured by mercury intrusion porosimetry and estimated specific surface area is shown in Figure 9. Although there is a strong negative correlation in the case of mullite-rich particles, no significant correlation is found in the case of Al-Si amorphous particles. Thus, the specific surface area of mullite-rich particles is considered to be a key parameter for the suppressing effect of ASR in FA.

4 CONCLUSIONS

In this study, feature analysis was carried out for five different FA having varied levels of the suppressing effect of ASR based on FE-SEM with various functions. From those results, the relation between FA characteristics and the suppressing effect of ASR was examined.

1) FE-SEM with EBSD/BSE/EDS successfully characterized FA particles (low Ca and alkali type) based on the measured geometrical parameters (particle shape, etc.) and chemical composition.

2) Feature analysis classified FA particles into six types. In addition, it was revealed that amorphous materials contain a large amount of phases in various textures.

3) A strong negative correlation was confirmed between 14-day expansion ratio and the estimated specific surface area of mullite-rich glass in the foreign alkali environment (ASTM C 1260).

4) Amorphous phases contained in mullite-rich glass is regarded to be the key factor for greatly contributing to the suppressing effect of ASR in FA.

5 REFERENCES

[1] Kawabata, Y, Matsushita, H (2007): Experimental study on the alkali silica reaction suppressing effect of fly ash mixed replacing fine aggregate. Concrete Science and Technology (18): 67-77. (in Japanese)

[2] Shehata, MH, Thomas, MDA (2000): The effect of fly ash composition on the expansion of concrete due to alkali-silica reaction. Cement and Concrete Research (30): pp.1063-1072.

[3] Malvar, LJ, Lenke, LR (2006): Efficiency of fly ash in mitigating alkali-silica reaction based on chemical composition. ACI Materials Journal (103): 319-326.

[4] Nagataki, S, Ohga, H, Inoue, T (1990): Suppressing effect of alkali aggregate reaction by fly ash and its mechanism. Journal of JSCE (414/V-12): 175-184. (in Japanese)

[5] Nambu, M, Tanosaki, T, Hayashi, K, Yamamoto, T, Ishikawa, Y (2007): Pozzolan performance evaluation of industrial by-products such as fly ash. Proc. of Waste materials (18): 143-146. (in Japanese)

[6] Williams, PJ, Biernacki, JJ, Rawn, CJ, Waker, L, Bai,J (2005): Microanalytical and computiational analysis of class F fly ash. ACI Material Journal (102):330-337.

[7] Kutchko, BG, Kim, AG (2006): Fly ash characterization by SEM-EDS. Fuel (85): 2537-2544.

[8] Chancey, RT, Stutzman, P, Juenger, CG, Flowler, DW (2010): Comprehensive phase characterization of crystalline and amorphous phases of a Class F fly ash. Cement and Concrete Research(40):146-156

[9] Enaga, Y, Aoto, N (2005): Change of magnetic properties and metal texture of SUS304 steel by high temperature damage. Zairyo (54): 116-121. (in Japanese)

[10] Shimizu, K, Torii, T, Mori, T (2005): Quantification method of the change of crystal orientation accompanied by fatigue of metal membrane material. Zairyo (54): 1041-1046. (in Japanese)

[11] Standard Test Methods for Rating and Classifying Inclusions in Steel Using the Scanning Electron Microscope, ASTM E 2142-08.

[12] Hoshino, H, Hirao, H, Yamada, K(2006): XRD/Rietveld Analysis of the Hydration and Strength Development of Slag and Limestone Blended Cement. Journal of Advanced Concrete Technology (4):357-367

[13] Berube, MA, Duchesne, J, Chouinard, D (1995): Why the accelerated mortar bar ASTM C 1260 is reliable for evaluating the effectiveness of supplementary cementing materials in suppressing expansion due to Alkali-silica reactivity. Cement, Concrete and Aggregate (17): 26-34.

[14] Igarashi, S, Tazaki, Y, Watanabe, A (2005): Estimation of water to cement ratio based on the evaluation of particle size distribution of remained unreacted cement particles. Concrete Science and Technology (16): 87-95. (in Japanese)

[15] Umezaki, A, Enomoto, M (2000): Estimation of number of precipitate particles per unit volume from measurements on polished specimen surfaces-computer simulation. ISIJ International (40): 1142-1148.

[16] Hayashi, K, Kono, K, Yamada, K (2009): Alkali silica reaction suppressing effect of fly ash type II under alkali supplying environments. Journal of Taiheiyo Cement Research (157): 11-21. (in Japanese)

TABLE 1: Chemical composition of FA

Sample	Chemical Composition (mass%)													
	LOI	SiO_2	Al_2O_3	Fe_2O_3	CaO	MgO	SO_3	Na_2O	K_2O	TiO_2	P_2O_5	MnO	Na_2O_{eq}	Total
FA-a	1.9	59.1	24.7	6.1	2.4	0.8	0.3	0.6	1.5	1.1	0.5	0.1	1.5	99.0
FA-b	1.9	56.3	28.2	4.8	2.9	1.2	0.4	0.7	1.3	1.5	0.3	0.0	1.5	99.4
FA-c	1.8	58.6	29.8	3.8	1.6	0.7	0.1	0.3	0.4	1.8	0.3	0.0	0.5	99.1
FA-d	2.4	70.2	19.1	2.7	1.5	0.5	0.2	0.5	1.1	0.9	0.3	0.0	1.2	99.4
FA-e	2.0	64.0	22.7	5.2	1.7	0.7	0.2	0.4	1.0	1.1	1.4	0.1	1.1	99.3

TABLE 2: Mineral composition of FA

Sample	LOI	α-quartz	Mullite	Magnetite	Hematite	Lime	Gypsum	Amorphous	Total
FA-a	1.9	6.3	12.4	0.7	0.0	0.0	0.6	78.2	100.1
FA-b	1.9	6.8	15.3	0.4	0.0	0.0	0.0	75.6	100.0
FA-c	1.8	7.6	13.9	0.8	0.0	0.0	0.0	75.6	100.1
FA-d	2.4	11.3	12.1	0.4	0.0	0.0	0.0	73.7	99.9
FA-e	2.0	14.6	14.5	0.8	0.0	0.0	0.0	68.1	100.0

TABLE 3: Chemical composition of amorphous phase

Sample	SiO_2	Al_2O_3	Fe_2O_3	CaO	MgO	SO_3	Na_2O	K_2O	TiO_2	Na_2Oeq	Total
FA-a	64.1	20.6	7.4	2.8	1.1	0.0	0.7	1.9	1.4	2.0	100.0
FA-b	60.4	23.0	6.0	3.8	1.6	0.5	0.9	1.7	2.0	2.0	99.9
FA-c	63.2	26.6	4.3	1.6	0.9	0.2	0.4	0.5	2.4	0.7	100.1
FA-d	76.0	14.3	3.3	2.1	0.7	0.2	0.7	1.5	1.2	1.6	100.0
FA-e	67.3	18.2	6.8	2.5	1.1	0.3	0.7	1.4	1.6	1.6	99.9

TABLE 4: Physical characteristics of FA

	Density g/cm^3	Blaine cm^2/g	Diameter μm	Reactivity index	
				28d	91d
FA-a	2.34	3890	15.1	84	100
FA-b	2.31	3490	18.7	83	98
FA-c	2.24	3590	31.0	82	99
FA-d	2.27	3780	17.4	84	100
FA-e	2.30	3670	19.5	82	98

TABLE 5: Threshold values for FA particle classification

Class	EDS quantification (mass%)				
	SiO_2	Al_2O_3	Fe_2O_3	CaO	TiO_2
α-quartz	>95	<5	<5	<5	<5
Fe rich	—	—	>25	—	—
Ti rich	—	—	—	—	>25
Mullite rich	25-90	>25	—	<25	—
Al-Si amorph.	25-90	<25	—	<25	—
Al-Si-Ca amorph.	25-90	<25	—	>25	—

TABLE 6: Particles numbers of each phase in FA classified by feature analysis								
	α-quartz	Fe rich	Ti rich	Mullite- rich	Al-Si amor.	Al-Si-Ca amor.	Non-classified	Total
FA-a	137	0	2	568	262	31	0	1000
FA-b	90	4	3	698	178	27	0	1000
FA-c	48	5	2	760	145	35	5	1000
FA-d	355	8	1	294	339	3	0	1000
FA-e	192	7	3	444	351	2	1	1000

TABLE 7: Average particles size and volume fraction of classified FA particles							
	Average particle size (μm)				Volume fraction (vol%)		
	Total	α-quartz	Al-Si glass	Mullite- rich	α-quartz	Al-Si glass	Mullite- rich
FA-a	20	16	10	15	12	13	45
FA-b	33	45	33	35	5	29	65
FA-c	40	19	14	42	3	9	77
FA-d	12	10	12	10	3	40	29
FA-e	15	8	12	15	9	26	56

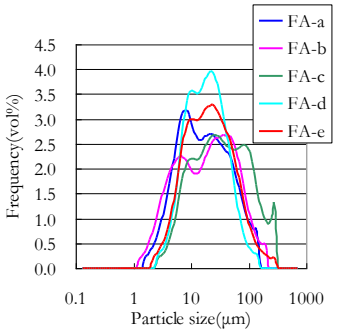

FIGURE 1: Particle size distribution of FA

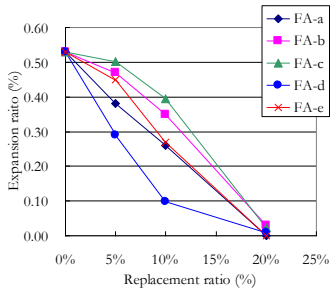

FIGURE 2: FA replacement ratio and 14 d expansion

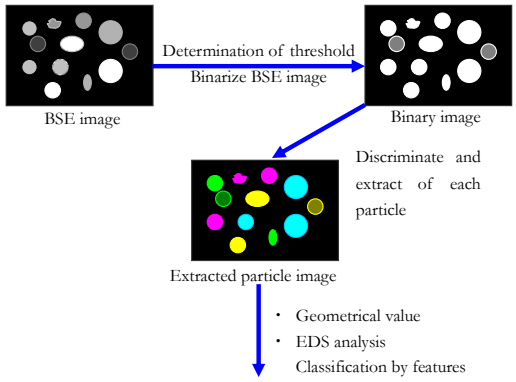

Class	Number	Area	Diameter	Gray Level	Chemcal compositions (mass%)			
					Si	Al	Ca	Fe
A	・・・			・・・	・・・	・・	・・・	・・
B	・・・			・・・	・・	・・	・・・	・・
C	・・・			・・・	・・	・・	・・・	・・
・・・	・・・			・・・	・・	・・	・・	・・

FIGURE 3: Flow diagram of feature analysis

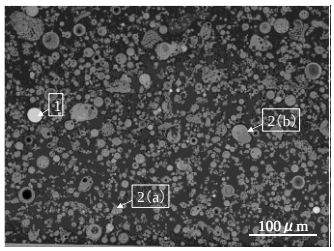

FIGURE 4: BSE image of FA-d (×250)

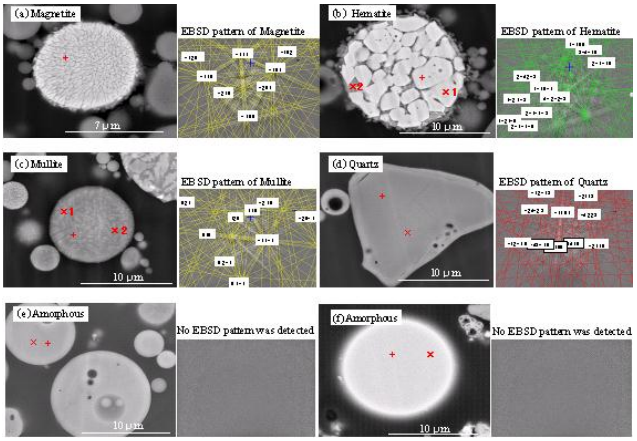

FIGURE 5: BSE images and EBSD patterns of FA particles (+: EBSD, numbers are face index, ×: EDS)

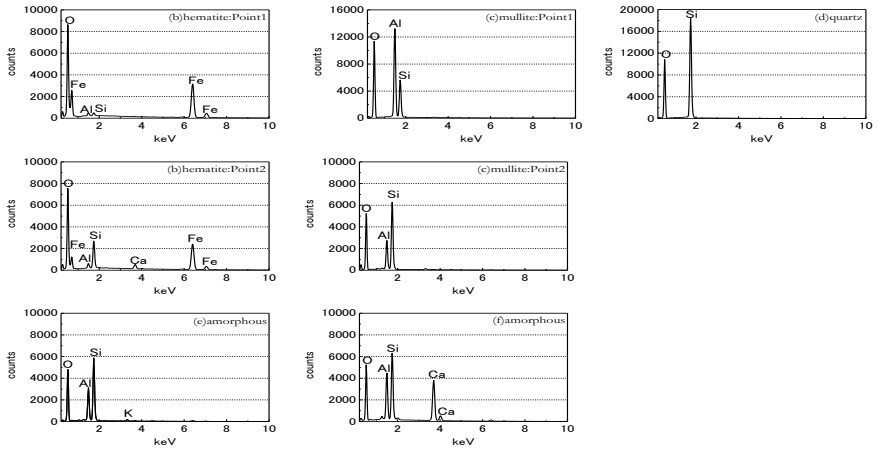

FIGURE 6: EDS spectrums of FA particles (analyzed points are indicated in Figure 5)

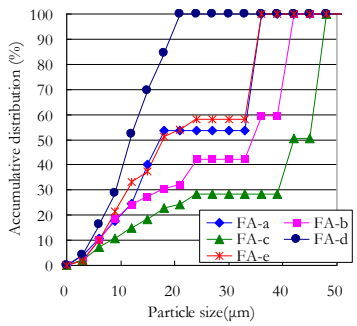

FIGURE 7: Estimated particle size distribution of mullite –rich particles

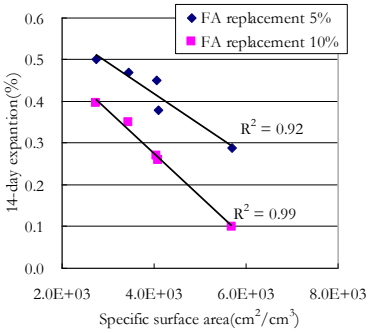

FIGURE 8: Estimated specific surface area of mullite-rich particles and 14-day expansion

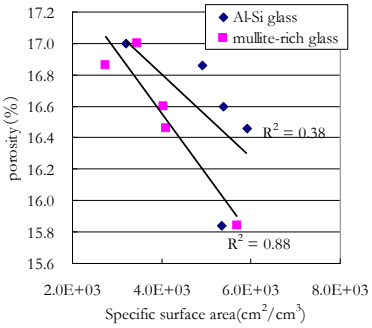

FIGURE 9: Estimated specific surface area and porosity of paste (FA=10%)